Orbital Analogue of the Quantum Anomalous Hall Effect in p-Band Systems

Congjun Wu

Department of Physics, University of California, San Diego, California 92093, USA

(Received 23 May 2008; published 31 October 2008)

We investigate the topological insulating states of the p-band systems in optical lattices induced by the on site orbital angular momentum polarization, which exhibit gapless edge modes in the absence of Landau levels. This effect arises from the energy-level splitting between the on site $p_x + ip_y$ and $p_x - ip_y$ orbitals by rotating each optical lattice site around its own center. At large rotation angular velocities, this model naturally reduces to two copies of Haldane's quantum Hall model. The distribution of the Berry curvature in momentum space and the quantized Chern numbers are calculated. The experimental realization of this state is feasible.

DOI: 10.1103/PhysRevLett.101.186807 PACS numbers: 73.43.Nq, 03.75.Ss, 05.50.+q

The precise quantization of the Hall conductance in the integer quantum Hall (QH) effect is due to the topologically nontrivial band structure characterized by the Thouless–Kohmoto–Nightingale–den Nijs (TKNN) number, or the Chern number [1,2]. The origin of the QH effect is also deeply connected to the parity anomaly of 2D Dirac fermions [3–5]. Although breaking time-reversal (TR) symmetry is required for the QH effect, Landau levels (LL) are not necessary. For example, Haldane [5] constructed a QH model with an average zero flux per unit cell but with complex-valued hopping integrals. QH insulators have been generalized to the topological quantum spin Hall (QSH) insulators which keep TR symmetry and are characterized by a Z_2 topological number [6–14].

The anomalous Hall effect describes the dependence of the Hall current on the spin magnetization, not the external magnetic field, whose mechanism has been debated for a long time, including the anomalous velocity from the interband matrix elements [15], the screw scattering [16], and the side jump [17]. Recently, a new perspective has been developed from the topological band Berry curvature [18,19]. Its quantum version, topological insulators arising from spin magnetization, has been proposed and investigated in semiconductor systems [20–22].

The development of cold atom physics has provided another new opportunity for the study of the QH effect. Several methods have been proposed including globally rotating the trap or optical lattice, or introducing effective gauge potential generated by laser beams [23–27]. Recently, a construction of Haldane's model has also been proposed [25] by superposing a periodic light-induced gauge potential with a honeycomb optical lattice.

In this article, we propose an orbital analogue of the quantum anomalous Hall (QAH) effect in solid state systems, i.e., the QAH effect arising from orbital angular momentum polarization without LLs. This can be achieved by rotating each optical site around its own center. The lift of the degeneracy between $p_x \pm ip_y$ orbitals gives rise to nontrivial topological band structures and provides a natural way to realize Haldane's model. Increasing rotation angular velocity induces topological phase transition by changing the Chern numbers of the band structure. We also present the study of the QH effect arising with LLs in this system.

We study the $p_{x,y}$-orbital band with spinless fermions in the honeycomb lattice described in Ref. [28–30] with the new ingredient of rotation as

$$\begin{aligned} H_0 &= t_{\parallel}\sum_{\vec{r}\in A}\{p^{\dagger}_{\vec{r},i}p_{\vec{r}+a\hat{e}_i,i} + \text{H.c.}\} - \mu\sum_{\vec{r}} n_{\vec{r}}, \\ H_L &= i\Omega_z\sum_{\vec{r}}\{p^{\dagger}_{\vec{r},x}p_{\vec{r},y} - p^{\dagger}_{\vec{r},y}p_{\vec{r},x}\}, \end{aligned} \tag{1}$$

where $\hat{e}_{1,2} = \pm\frac{\sqrt{3}}{2}\hat{e}_x + \frac{1}{2}\hat{e}_y$ and $\hat{e}_3 = -\hat{e}_y$ are the unit vectors pointing from a site in the A-sublattice to its three neighbors in the B-sublattice; $p_i \equiv (p_x\hat{e}_x + p_y\hat{e}_y)\cdot\hat{e}_i (i = 1\text{–}3)$ are the projections of the p-orbitals along the $\hat{e}_i$ direction; μ is the chemical potential; a is the nearest-neighbor bond length. Since there is no overall lattice rotation, the vector potential due to the Coriolis force and the centrifugal potential across the entire lattices do not appear. The effect is to break the degeneracy between $p_x \pm ip_y$ as described by H_L.

The band structure of Eq. (1) is presented as follows. Under the chiral transformation C, i.e., $p_{r_A,x,y} \rightarrow p_{r_A,x,y}$, $p_{r_B,x,y} \rightarrow -p_{r_B,x,y}$, combined by the time-reversal transformation T, Eq. (1) transforms as $(CT)^{-1}(H_0 + H_L)\times(CT) = -(H_0 + H_L)$; thus, its spectra are symmetric respect to the zero energy. At $\Omega_z = 0$, it exhibits two dispersive bands touching at Dirac cones located at $K_{1,2} = (\pm\frac{4\pi}{3\sqrt{3}a}, 0)$ and other two flat bands [28,29]. The dispersive bands touch the flat bands at the Brillouin zone (BZ) center $K_0 = (0, 0)$. At nonzero Ω_z, gaps open between different bands as depicted in Figs. 1(a)–1(c). If Ω_z is small, the effective Hamiltonian close to the Dirac points of $K_{1,2}$ becomes massive with the gap value of $\Delta = \Omega_z$. The masses at $K_{1,2}$ are of opposite signs. The bottom band is no longer flat at nonzero Ω_z. Its minimum at K_0 is pushed down by the value of $\frac{3}{2}\Omega_z$ and that of the second band is pushed up by the same value. This opens a gap of

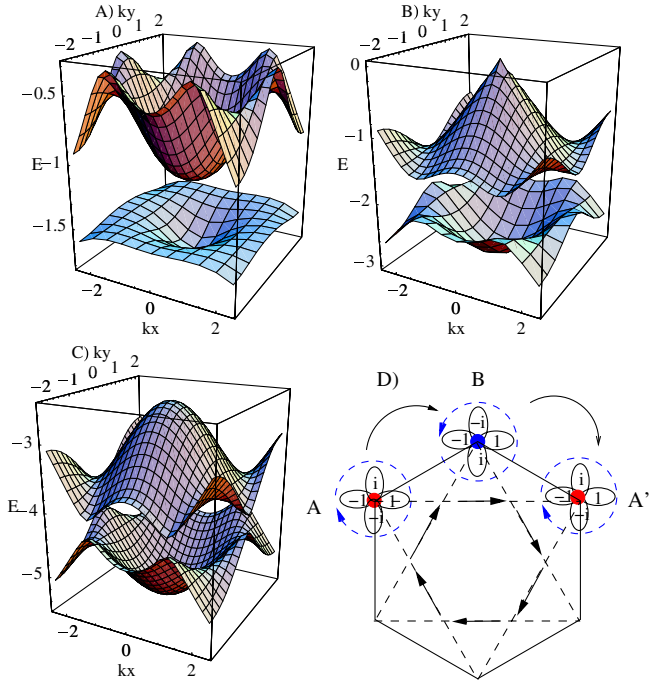

FIG. 1 (color online). The band structure of Eq. (1) at $\Omega_z > 0$ as shown in (a), (b), and (c). Only the lower two bands are presented, and the upper two are symmetric respect to the zero energy. (a) $\Omega_z/t_\parallel = 0.3$; (b) $\Omega_z/t_\parallel = 1.5$ where a single gapless Dirac cone appears; (c) $\Omega_z/t_\parallel = 3$ where two massive Dirac cones appear at $K_{1,2}$ between the lower two bands and also between the upper two bands; (d) The pattern of the induced NNN hopping (complex valued) at $\Omega_z \gg t_\parallel$, which is generated by the virtual hopping between orbitals with opposite chirality.

$3\Omega_z$. A similar analysis applies to the top and the third bands.

As Ω_z approaches $\frac{3}{2}t_\parallel$, the middle two bands at K_0 are pushed to zero from both up and below, respectively. A single gapless Dirac cone is formed at the BZ center $K_0 = (0, 0)$ as depicted in Fig. 1(b). We define the four-component spinor as $\psi = (p_{x,A}, p_{y,A}, p_{x,B}, p_{y,B})^T$, and two bases of $\phi_1 = \frac{1}{2}\{1, i, -1, -i\}$ and $\phi_2 = \frac{1}{2} \times \{1, -i, 1, -i\}$ for the middle two bands. The Dirac cone Hamiltonian at K_0 can be expressed as

$$H_2(\vec{k}) = \begin{pmatrix} -(\Omega_z - \frac{3}{2}t_\parallel) & -\frac{3}{2}t_\parallel(k_x + ik_y) \\ -\frac{3}{2}t_\parallel(k_x - ik_y) & \Omega_z - \frac{3}{2}t_\parallel \end{pmatrix}. \quad (2)$$

We notice that a single Dirac cone of the chiral fermion is allowed in the 2D bulk lattice systems, which actually does not contradict to the fermion doubling theory proved for 3D lattices [31].

As Ω_z goes even larger, the lower and upper two pairs of bands are projected into the single orbital bands of $p_x \pm ip_y$, respectively. The lower two are described by the $p_x + ip_y$ orbital with a nearest-neighbor hopping of $\frac{t_\parallel}{2}$. Furthermore, a Haldane type NNN hopping is generated as depicted in Fig. 1(d): one particle at site A in the $p_x + ip_y$ orbital hops to the high energy orbital of $p_x - ip_y$ at its nearest neighbor B, and hops back into the $p_x + ip_y$ state at the NNN site A'. Along the directions indicted by arrows, this hopping amplitude can be calculated from the second order perturbation theory as $t_{nn} = t_\parallel^2/(2\Omega_z)e^{i(2/3)\pi}$. As pointed out in Ref. [5], this generates two massive Dirac cones with gap $\Delta = \frac{9}{2}t_{nn}$ at $\vec{K}_{1,2}$ of masses with opposite signs.

The above bands exhibit nontrivial topological properties. Let us label the four bands with indices from 1 to 4 as energy increases. The Berry curvature $F_{n,xy}(\vec{k})$, or the gauge field strength, in the momentum space for the n-th band is defined as $F_{n,xy}(\vec{k}) = \partial_{k_x}A_{n,y}(\vec{k}) - \partial_{k_y}A_{n,x}(\vec{k})$, where $A_{n,\mu}(\mu = x, y)$ is the gauge potential defined as $A_{n,\mu} = i\langle\psi_n(\vec{k})|\partial_{k_\mu}|\psi_n(\vec{k})\rangle$ [1,2]. The eigenstates of different bands are related by the combined chiral and TR transformation as $|\psi_4(-\vec{k})\rangle = (TP)|\psi_1(\vec{k})\rangle$ and $|\psi_3(-\vec{k})\rangle = (TP)|\psi_2(\vec{k})\rangle$; thus, the Berry curvatures of different bands satisfy $F_{4,xy}(-\vec{k}) = -F_{1,xy}(\vec{k})$ and $F_{3,xy}(-\vec{k}) = -F_{2,xy}(\vec{k})$. $F_{n,xy}$ of the lower two bands is depicted in Fig. 2 at different angular velocities. The total flux in the BZ for the n-th band is quantized known as the Chern number $C_n = \frac{1}{2\pi}\int d^2k F_{n,xy}(\vec{k})$ [1,2]. At all values of $\Omega_z > 0$, C_1 is quantized to 1, in spite of a significant change of distribution of $F_{1,xy}$ as increasing Ω_z as depicted in Figs. 2(a), 2(c), and 2(e). The maximal of $F_{1,xy}$ are

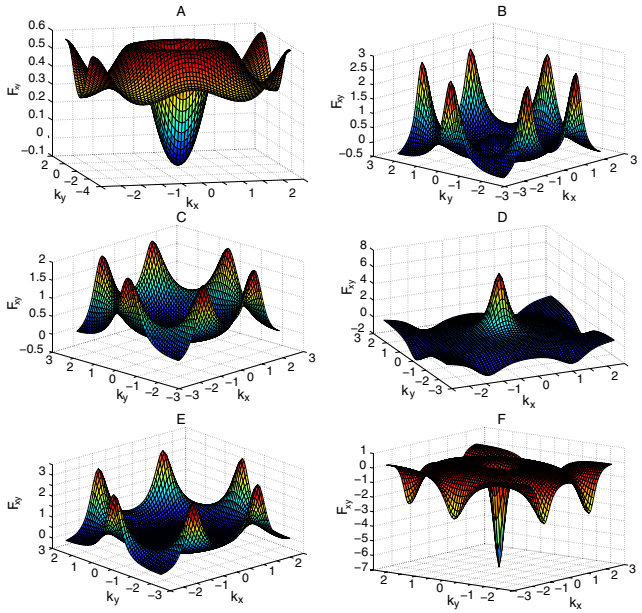

FIG. 2 (color online). The distribution of the Berry curvature $F_{n,xy}(\vec{k})$ in the Brillouin zone for the lower two bands at different Ω_z. (a), (c), and (e) [(b), (d), and (f)] are $F_{n,xy}(\vec{k})$ of the first (second) band at $\Omega_z/t_\parallel = 0.3$, 1.3 and 1.7, respectively. The Chern number of the first band is 1, and that of the second band changes from 0 to -1 at $\Omega_z/t_\parallel = \frac{3}{2}$.

distributed among a ring around the BZ center at small values of Ω_z, and are pushed to the two vertexes of the BZ at $K_{1,2}$ as Ω_z increases. C_2 is more subtle. At small Ω_z, each of two massive Dirac points at $K_{1,2}$ approximately contribute a flux of $\frac{1}{2}$. As $\Omega_z/t_\parallel \to \frac{3}{2}$ from below, the maximum of $F_{2,xy}$ is shifted to the new Dirac point at the BZ center, which approximately contributes the flux of $\frac{1}{2}$. However, these contributions are canceled by the background negative flux $-\frac{1}{2}$ when $\Omega_z/t_\parallel < \frac{3}{2}$, and thus the Chern number is 0. A topological quantum phase transition occurs at $\Omega_z/t_\parallel > \frac{3}{2}$ beyond which the flux from the Dirac point K_0 flips the sign to $-\frac{1}{2}$. Combined with the background contribution $-\frac{1}{2}$, the Chern number of C_2 changes to -1. In analogy to electron systems, the transverse conductivity can be defined as the ration between the mass flow and the potential gradient as $\sigma_{xy} = -J_x/\partial_y V$.

The above band structure gives rise to topological stable gapless edge modes lying inside the band gap. Figure 3 depicts the spectra with the open boundary condition on the zigzag edges. When the Fermi level lies in the band gap between the nth and $n+1$th bands, σ_{xy} is quantized as the sum of the Chern numbers of the occupied bands as $\sigma_{xy}(n, n+1) = \frac{m}{\hbar}\sum_{1\sim n} C_i$ [1,2], which is just the number of the chiral edge modes inside the gap. At $\Omega_z < \frac{3}{2}t_\parallel$, the Chern numbers reads $C_1 = -C_4 = -1$ and $C_2 = -C_3 = 0$, giving rise to $\sigma_{xy}(n, n+1)/(\frac{m}{\hbar}) = 1$ for $n = 1, 2, 3$. Thus, edge modes exist in all of the three band gaps with the same chirality. At $\Omega_z > \frac{3}{2}t_\parallel$, C_2 and C_3 change to $C_2 = -C_3 = -1$, giving rise to $\sigma_{xy}(n, n+1)/(\frac{m}{\hbar}) = 1, 0, -1$ for $n = 1, 2, 3$. Thus, the edge modes between bands 1 and 2 and that between band 3 and 4 are of the opposite chiralities. No edge mode appears between band 2 and 3. This agrees with the picture that Eq. (1) reduces to two copies of Haldane's model at $\Omega_z \gg t_\parallel$.

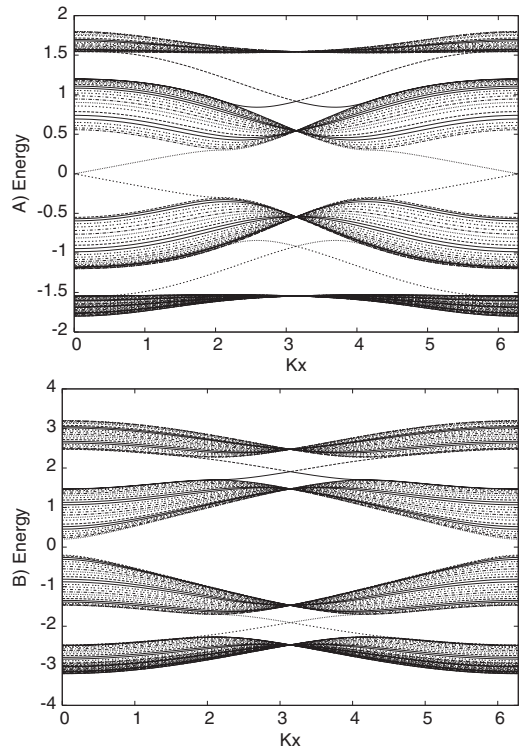

FIG. 3. The gapless edge excitations with the open boundary condition along the zigzag edge of the hexagon lattice. (a) $\Omega_z/t_\parallel = 0.3$; (b) $\Omega_z/t_\parallel = 1.7$. A topological phase transition occurs at $\Omega_z/t_\parallel = \frac{3}{2}$ above which the edge modes between the middle two bands disappear.

We also study the QH effect of Eq. (1) arising from LLs by replacing the hopping part to

$$H_{\text{hop}} = t_\parallel \sum_{\vec{r}\in A} \{p^\dagger_{\vec{r},i} p_{\vec{r}+a\hat{e}_i,i} e^{i\int_{r+ae_i}^{r} \vec{A}\cdot d\vec{r}} + \text{H.c.}\}, \qquad (3)$$

where the vector potential-$\vec{A}$ can be generated through another overall lattice rotation or by light-induced gauge potential. We will take the flux per plaquette Φ and Ω_z as two independent variables. The spectra of the above Hamiltonian does not depend on the gauge choice, but the physical wave functions differ by a gauge transformation. For the calculation convenience, we use the Landau gauge for an open boundary system along the zigzag edge and take $\Phi/(2\pi) = 0.05$.

In the presence of $\vec{A}$, $(CP)(H_{\text{hop}} + H_L)(CP)^{-1} \neq -(H_{\text{hop}} + H_L)$; thus, the spectra are no longer symmetric respect to the zero energy. Generally speaking, all of the four bands split into a number of flat LLs with dispersive edge modes lie in between. The pattern of edge modes does not change much as varying the value of Φ, but significantly changes as increasing Ω_z. At small values of Ω_z [e.g., $\Omega_z = 0.2t_\parallel$ as shown in Fig. 4(a)], gapless edge modes go through the entire spectra from the very band bottom to top. Landau levels close to the zero energy arise from Dirac cones at $K_{1,2}$ with opposite masses. The 0th LL is pushed to the negative energy at the gap value around $-0.26t_\parallel$. The number of chiral edge modes between levels of $n = 0$ and ± 1 is 1 with opposite chirality and that between $n = \pm 1$ and ± 2 is 3. The energies of $n = \pm 1$ and $n = \pm 2$ appear roughly symmetric to zero energy. All of these agree with the picture of LLs from two massive Dirac cones. Next, let us look at $\Omega_z = \frac{3}{2}t_\parallel$ where a single gapless Dirac cone appears as shown in Eq. (2). Indeed, the 0th LL appears close to the zero energy but with a small deviation, which is understandable as no exact symmetry to protect it right at the zero energy. It is tempting to think the appearance of the half-integer QH effect, but this is impossible in free-lattice fermion systems [5]. Another half has to be contributed from the high energy part of the band structure. As a result, the number of chiral edge modes between LLs $n = 0$ and 1 is $\frac{1}{2} + \frac{1}{2} = 1$, while that between LLs $n = 0$ and -1 is $-\frac{1}{2} + \frac{1}{2} = 0$. Thus, the spectra from bottom to top become disconnected without edge modes connecting them. This disconnection actually begins to appear even earlier at $\Omega_z = 1.2t_\parallel$, and is enhanced as Ω_z goes larger. At large values of Ω_z, the model

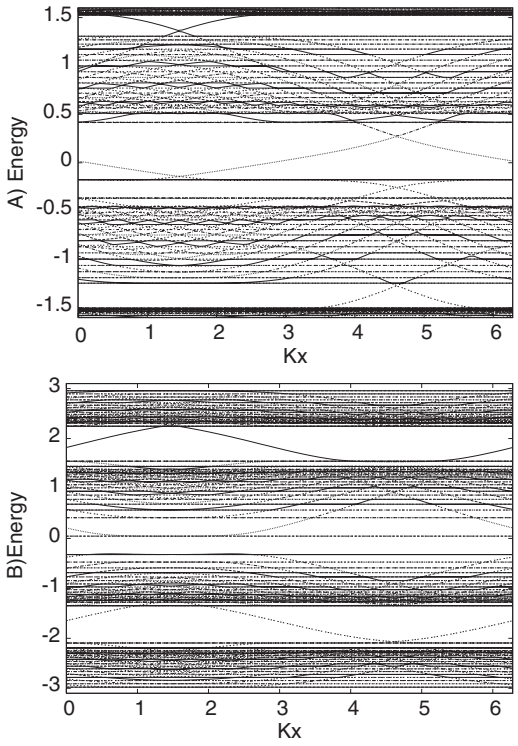

FIG. 4. Edge and bulk states spectra of Eq. (3) with the open boundary condition along the zigzag edge. The flux per plaquette $\phi/(2\pi) = 1/20$. (a) $\Omega_z/t_\parallel = 0.2$; (b) $\Omega_z/t_\parallel = 1.5$.

reduces to two copies ($p_x \pm ip_y$) of Haldane's model. The patterns of LLs between bands 1 and 2, and between bands 3 and 4 become those of the two massive Dirac cones with opposite mass signs. When Fermi level lies in between LLs, the transverse conductance σ_{xy} is quantized at the value of the number of chiral edge modes.

The experimental techniques to realize QAH insulators are basically available. Spinless fermions can be realized by polarized ^{6}Li or ^{40}K atoms. The honeycomb optical lattice was constructed quite some time ago [32]. The rotation of each lattice site around its own site center has been performed by Gemelke *et al.* [33] as follows. Electro-optic phase modulators are applied to the laser beams forming the lattice. This results in an oscillation of the overall lattice translation at a radio frequency which is much larger than the harmonic frequency of each site; thus, atoms only feel an averaged potential with a small distortion along the oscillation axis. This axis is controlled to rotate at an audio frequency Ω_z, which induces the rotation of each site around its own center. Ω_z can be tuned from zero to a few kHz, which is at the order of the recoil energy E_R corresponding to the temperature scale of 0.1 μK and is experimentally realizable. An application of such method to the hexagonal lattice is expected feasible. As calculated in Ref. [29], by varying laser intensity $t_\parallel$ can be easily tuned from the same order of E_R to one order smaller; thus, we have a large flexibility to tune $\Omega_z/t_\parallel$. QAH insulators are still band insulators, and thus are robust at temperatures small compared to band gaps. Band gaps are comparable to $t_\parallel$ as shown in Fig. 3, which can be tuned to the order of E_R; thus, the temperature scale to realize QAH insulators is experimentally realizable. The direct detection of QAH insulators through transport measurement in cold atom experiments might be difficult, and a recent proposal based on the Streda formula through the time of flight measurement of particle density has been provided in Ref. [26].

In summary, we investigate the topological insulating states in the p-orbital systems in the honeycomb lattice. The orbital angular momentum polarization generates the nontrivial Chern number structure giving rise to the orbital counterpart of QAH effect without LLs. QH effect arising for LLs are also investigated, which shows quantitative different features from those in graphene.

C. W. thanks D. Arovas, M. Fogler, and J. Hirsch for helpful discussions, and N. Gemekel for the introduction of the method of rotating optical lattices. C. W. is supported by the Sloan Research Foundation, ARO-W911NF0810291, NSF No. DMR-0804775, and the Academic Senate research grant at UCSD.

[1] D. J. Thouless *et al.*, Phys. Rev. Lett. **49**, 405 (1982).
[2] M. Kohmoto, Ann. Phys. (N.Y.) **160**, 343 (1985).
[3] R. Jackiw, Phys. Rev. D **29**, 2375 (1984).
[4] E. Fradkin *et al.*, Phys. Rev. Lett. **57**, 2967 (1986).
[5] F. D. M. Haldane, Phys. Rev. Lett. **61**, 2015 (1988).
[6] B. A. Bernevig *et al.*, Science **314**, 1757 (2006).
[7] X.-L. Qi *et al.*, arXiv.org:0802.3537 [Phys. Rev. B (to be published)].
[8] C. L. Kane *et al.*, Phys. Rev. Lett. **95**, 146802 (2005).
[9] J. E. Hirsch, Phys. Rev. B **40**, 2354 (1989).
[10] D. N. Sheng *et al.*, Phys. Rev. Lett. **97**, 036808 (2006).
[11] J. E. Moore *et al.*, Phys. Rev. B **75**, 121306 (2007).
[12] R. Roy, arXiv:cond-mat/0604211.
[13] M. König *et al.*, Science **318**, 766 (2007).
[14] D. Hsieh *et al.*, Nature (London) **452**, 970 (2008).
[15] R. Karplus *et al.*, Phys. Rev. **95**, 1154 (1954).
[16] J. Smit, Physica (Amsterdam) **24**, 39 (1958).
[17] L. Berger, Phys. Rev. B **2**, 4559 (1970).
[18] T. Jungwirth *et al.*, Phys. Rev. Lett. **88**, 207208 (2002).
[19] N. Nagaosa, J. Phys. Soc. Jpn. **75**, 042001 (2006).
[20] X.-L. Qi *et al.*, Phys. Rev. B **74**, 085308 (2006).
[21] C.-X. Liu *et al.*, Phys. Rev. Lett. **101**, 146802 (2008).
[22] M. Onoda *et al.*, Phys. Rev. Lett. **90**, 206601 (2003).
[23] T. L. Ho and S. K. Yip, Phys. Rev. Lett. **84**, 4031 (2000).
[24] V. W. Scarola *et al.*, Phys. Rev. Lett. **98**, 210403 (2007).
[25] L. B. Shao *et al.*, arXiv.org:0804.1850.
[26] R. O. Umucalilar *et al.*, Phys. Rev. Lett. **100**, 070402 (2008).
[27] S.-L. Zhu *et al.*, Phys. Rev. Lett. **97**, 240401 (2006).
[28] C. Wu *et al.*, Phys. Rev. Lett. **99**, 070401 (2007).
[29] C. Wu *et al.*, Phys. Rev. B **77**, 235107 (2008).
[30] C. Wu, Phys. Rev. Lett. **100**, 200406 (2008).
[31] H. B. Nielsen *et al.*, Nucl. Phys. B **185**, 20 (1981).
[32] G. Grynberg *et al.*, Phys. Rev. Lett. **70**, 2249 (1993).
[33] N. Gemelke, Ph.D. thesis, Stanford University, 2007.